Toxicity of Graphene and Graphene Oxide Nanowalls Against Bacteria

Omid Akhavan*,[†],[‡] and Elham Ghaderi[†]

[†]Department of Physics, Sharif University of Technology, P.O. Box 11155-9161, Tehran, Iran, and [‡]Institute for Nanoscience and Nanotechnology, Sharif University of Technology, P.O. Box 14588-89694, Tehran, Iran

Graphene, as a single-atom-thick sheet of sp2-bonded carbon atoms in a closely packed honeycomb two-dimensional lattice, is one of the most fascinating nanostructures with unique physical, chemical, electrical, and mechanical properties which qualify it as a promising nanomaterial in condensed-matter and high-energy physics,[1−3] material science,[4−9] and a wide range of technological applications,[10−18] such as bioelectronics and biosensing.[19−21]

Some of the unique properties of graphene nanosheets are similar or even identical to the properties of carbon nanotubes (CNTs). Previous investigations have demonstrated that single-wall carbon nanotubes (SWCNTs) present a noticeable cytotoxicity to human[22−26] and animal cells,[27,28] while multiwall carbon nanotubes (MWCNTs) not only show a more moderate toxicity than SWCNTs,[26] but also sometimes act as suitable sites for proliferation of bacteria.[29] Among the suggested toxicity mechanisms including oxidative stress,[22,23,30−32] cutting off intracellular metabolic routes,[30] and rupture of cell membrane,[33] the oxidative stress has been regarded as the most acceptable mechanism explaining the toxicity of CNTs to mammalian cells. In addition to mammalian cells, bacteria, e.g. *Escherichia coli* (*E. coli*), can be also used as appropriate models to examine the toxicity of CNTs to such single-celled microorganisms.[34] In this regard, Kang et al. showed that the main CNT-cytotoxicity mechanism explaining inactivation of *E. coli* is direct contact interaction of the bacteria with highly purified CNTs.[33,35] Moreover, they demonstrated that the nanometric size of SWCNTs is responsible of their much stronger bactericidal activity than MWCNTs, in the mechanism of direct contact interaction of the bacteria with the CNTs.[35]

By extending this subject to graphene, the edges of graphene nanosheets with extremely high aspect ratio (the ratio of lateral size to the atomic thickness) can be proposed as one of the excellent and ideal nanostructures for an effective direct contact interaction with microorganisms. But, toxicity of graphene sheets, particularly the direct interaction of its extremely sharp edges with microorganisms, has not been studied, maybe due to the difficulties in fabrication of graphene nanowalls. So far, based on a few reports, it was found that graphene papers (not graphene nanowalls) are biocompatible materials,[36,37] the graphene and graphene oxide suspensions can inhibit the growth of *E. coli* bacteria but with a minimal cytotoxicity,[38] and graphene sheets can enhance photoinactivation of *E. coli* bacteria on the surface of graphene/TiO2 composite thin film.[39]

ABSTRACT Bacterial toxicity of graphene nanosheets in the form of graphene nanowalls deposited on stainless steel substrates was investigated for both Gram-positive and Gram-negative models of bacteria. The graphene oxide nanowalls were obtained by electrophoretic deposition of Mg^{2+}-graphene oxide nanosheets synthesized by a chemical exfoliation method. On the basis of measuring the efflux of cytoplasmic materials of the bacteria, it was found that the cell membrane damage of the bacteria caused by direct contact of the bacteria with the extremely sharp edges of the nanowalls was the effective mechanism in the bacterial inactivation. In this regard, the Gram-negative *Escherichia coli* bacteria with an outer membrane were more resistant to the cell membrane damage caused by the nanowalls than the Gram-positive *Staphylococcus aureus* lacking the outer membrane. Moreover, the graphene oxide nanowalls reduced by hydrazine were more toxic to the bacteria than the unreduced graphene oxide nanowalls. The better antibacterial activity of the reduced nanowalls was assigned to the better charge transfer between the bacteria and the more sharpened edges of the reduced nanowalls, during the contact interaction.
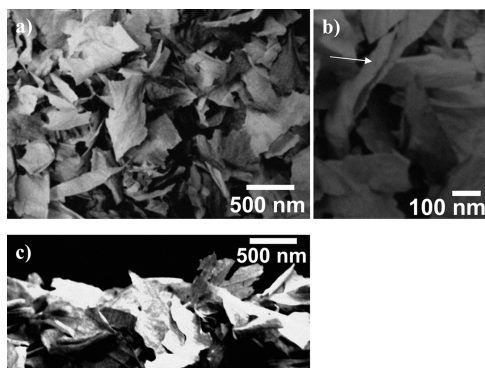
Figure 1. SEM images of (a) the GONWs deposited on stainless steel substrate by EPD, (b) the nanowalls at a higher magnification showing those are nearly perpendicular to the substrate, and (c) the cross-sectional view of the nanowalls.

Electrophoretic deposition (EPD) is an inexpensive and versatile technique for deposition of various coatings from various suspensions. In addition, EPD has presented many advantages in the deposition of different coatings including good surface homogeneity, easy control of film thickness, high deposition rate, no requirement to binders, and simplicity of scaling up. For instance, CNT coatings with good microstructural uniformity and high packing density were fabricated by EPD from colloidal CNT suspensions.[40,41] Recently, Wu et al.[42] fabricated single-layer graphene films by EPD from a stable suspension of isopropyl alcohol-dispersed graphene prepared by a chemical exfoliation. They demonstrated that the field-emission properties of the graphene films were much better than those of its graphene powder counterpart and well comparable or even better than those of CNTs.

In this work, at first, graphene oxide nanowalls (GONWs) were deposited on stainless steel substrates by using EPD from a suspension containing Mg^{2+}-graphene oxide nanosheets synthesized by a chemical exfoliation method. The synthesized GONWs were also reduced by hydrazine to obtain reduced graphene nanowalls (RGNWs). Then, the bacterial toxicity of the GONWs and the RGNWs was studied for the first time. To further investigate the mechanism of direct contact interaction of the nanowalls with bacteria, the RNA effluxes through the damaged cell membranes of both Gram-negative *E. coli* and Gram positive *Staphylococcus aureus* (*S. aureus*) bacteria were examined.
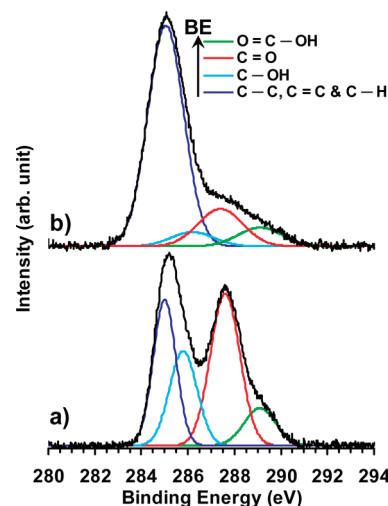

Figure 2. Peak deconvolution of C(1s) XPS core level of (a) the GONWs and (b) the RGNWs.

RESULTS AND DISCUSSION

Figure 1 shows scanning electron microscope (SEM) images of the GONWs obtained by EPD on the stainless steel substrate. It is seen that single- and/or multilayer graphene oxide sheets were deposited in high-density and random orientations, but some of them are almost perpendicular to surface of the substrate. These nearly perpendicular sheets provided extremely sharp edges on the surface. Therefore, the bacteria can effectively interact with the graphene (oxide) nanosheets through direct contact with such sharp edges. It was also found that reducing the nanowalls by vapor of hydrazine could not change the morphology of the nanowalls.

To investigate the changes in the chemical states of the GONWs, X-ray photoelectron spectroscopy (XPS) was used. The deconvoluted C(1s) XPS spectra of the GONWs and the RGNWs have been presented in Figure 2. The binding energy of 285.0 eV was ascribed to the C—C, C=C, and C—H bonds on the surface of the sheets. The deconvoluted peaks centered at the binding energies of 285.8, 287.6, and 289.1 eV were attributed to the C—OH, C=O, and O=C—OH functional groups, respectively.[39,43−46] The contribution of the bonds was estimated by peak area ratios of the C—OH, C=O, and O=C—OH bonds to the C—C, C=C, and C—H bonds, as also listed in Table 1. It was found the reduction of the GONWs by hydrazine resulted in 89%, 84%, and 69% reduction in the peak area ratio of the

TABLE 1. The Peak Area (A) Ratios of the Oxygen-Containing Bonds to the CC Bonds (by XPS), the Peak Intensity Ratios of I_D/I_G (by Raman), and the Antibacterial Activity of the GONWs and the RGNWs

| | XPS | | | Raman | antibacterial activity | | | |
| | | | | | survival bacteria (%) | | RNA (ng/mL) | |
sample	A_{COH}/A_{CC}	A_{CO}/A_{CC}	A_{OCOH}/A_{CC}	I_D/I_G	*E. coli*	*S. aureus*	*E. coli*	*S. aureus*
GONWs	0.78	1.35	0.36	1.78	41 ± 8	26 ± 5	30 ± 4	38 ± 5
RGNWs	0.08	0.21	0.11	1.26	16 ± 3	5 ± 1	43 ± 6	56 ± 8
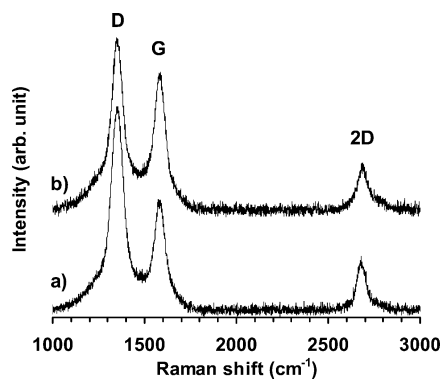
Figure 3. Raman spectra of (a) the GONWs and (b) the RGNWs.

Figure 4. Cytotoxicity of GONWs and RGNWs to *E. coli*, and concentrations of RNA in the PBS of the *E. coli* bacteria exposed to the nanowalls.
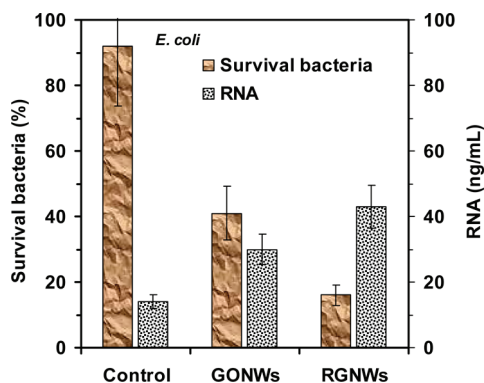
C—OH, C=O, and O=C—OH oxygen-containing functional groups, respectively. Therefore, the reduction process could effectively reduce the GONWs into graphene nanowalls.

To study the effect of the reduction process on the carbon structure of the GONWs, Raman spectroscopy was utilized, as shown in Figure 3. In fact, Raman spectroscopy is known as an efficient method to examine the ordered/disordered crystal structures of carbonaceous materials, such as graphene. The famous characteristics of Raman spectra of carbon materials are the D and G bands ($\sim$1350 and 1580 cm^{-1}) which are usually attributed to the local defects/disorders (especially located at the edges of graphene and graphite platelets) and the sp^2 graphitized structure, respectively.[47,48] Therefore, smaller I_D/I_G peak intensity ratios are assigned to lower defects/disorders in a graphitized structure such as graphene. The Raman spectra shown in Figure 3 display the D and G lines at about 1348 and 1575 cm^{-1}, respectively. The values of the I_D/I_G ratio were also estimated and also given in Table 1. The reduction process resulted in reduction of the I_D/I_G ratio from 1.78 for the GONWs to 1.26 for the RGNWs, indicating improvement in the graphitized structure of the nanowalls due to the reduction process. On the basis of analysis of Raman spectra, it is also possible to judge about the single-, bi-, and/or multi-layer structures of graphene and graphene oxide layers. For the G band, the peak position of the single-layer graphenes, typically centered at 1585 cm^{-1}, shifts into lower wavenumbers after stacking further graphene layers.[49−51] For example, for 2−6 layers the G band shifts 6 cm^{-1} into lower wavenumbers. In addition to the peak position of the G band, shape and position of the 2D band are known as the key parameters for determination of the layer numbers of graphene sheets.[49−52] For example, the 2D peak position of the single-layer graphene sheets (typically centered at 2679 cm^{-1}) shifts to higher wavenumbers by 19 cm^{-1} for multi-layer graphenes (2−4 layers).[48] In this work, the 2D bands of the GONWs were centered at 2682 cm^{-1} with a shoulder at the higher wavenumbers, indicating the GONWs were con-

stituted by single- and multi-layer graphene oxide sheets, consistent with the SEM observations. By reducing the GONWs, the 2D peak position slightly shifted to 2686 cm^{-1} and the intensity of the shoulder slightly increased. These changes can be attributed to slight aggregation of the initially overlapped sheets due the reduction process.

To investigate about bacterial toxicity of the GONWs and the RGNWs, *E. coli* and *S. aureus* bacteria were used as models for Gram-negative and Gram-positive bacteria. To have a bench mark, the bare stainless steel substrate was also used as a control sample. Bactericidal activity of the nanowalls against *E. coli* bacteria was presented in Figure 4. For the control sample, no considerable antibacterial activity was observed in our experimental conditions. But, the GONWs and particularly the reduced nanowalls exhibited considerable antibacterial activities. In fact, after 1 h, 41($\pm$8)% and 16($\pm$3)% of the bacteria could survive on the surface of the GONWs and the RGNWs, respectively. The antibacterial activity of the RGNWs is also comparable with the antibacterial activity of SWCNTs which can inactivate 87($\pm$7)% of *E. coli* bacteria in 1 h.[35]

Figure 5 shows similar study for *S. aureus* bacteria. Once again it was found that the nanowalls were toxic to the bacteria. But, the nanowalls exhibited stronger antibacterial activities against *S. aureus* bacteria than
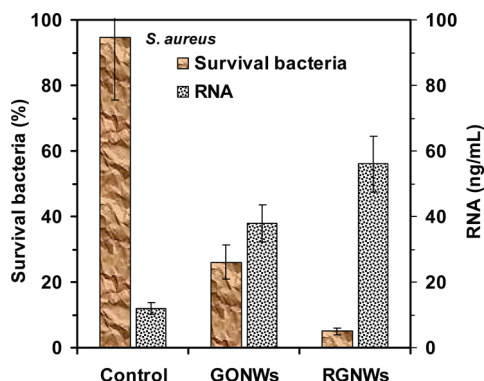

Figure 5. Cytotoxicity of GONWs and RGNWs to *S. aureus*, and concentrations of RNA in the PBS of the *S. aureus* bacteria exposed to the nanowalls.

their activities against *E. coli* bacteria. In fact, only 26(±5)% and only 5(±1)% of the bacteria could survive on the surface of the GONWs and the RGNWs after 1 h, respectively. Therefore, although the synthesized nanowalls were toxic to the both models of the bacteria (Gram-negative and Gram-positive models), they were more toxic to Gram-positive bacteria (here, *S. aureus* bacteria). In addition, for each model of the bacteria, the reduced nanowalls exhibited stronger toxicity than the oxide nanowalls.

The toxicity of the nanowalls through cell membrane damage of the bacteria can be investigated by measuring the intracellular materials in the phosphate buffer solution (PBS) of the bacteria exposed to the nanowalls. Concerning this, the efflux of cytoplasmic materials of the bacteria was examined by measuring the concentration of RNA in the solution as shown in Figures 4 and 5 for *E. coli* and *S. aureus* bacteria, respectively. The figures show that concentrations of RNA in the solutions of the bacteria exposed to the both GONWs and RGNWs were meaningfully higher than the RNA concentration of the control sample. This was attributed to direct contact of the bacterial cell, which has slightly negative charge with the edge of the nanowalls as good electron acceptors, and consequently, cell membrane damage of the bacteria. For each model of the bacteria, the cell membrane damage caused by the reduced nanowalls was substantially higher than the damage caused by the oxide nanowalls. This can be assigned to a stronger interaction between the more sharpened edges of the reduced nanowalls with the cell membrane of the bacteria and/or a better charge transfer between the bacteria and the edge of the reduced nanowalls which finally resulted in further damage of the cell membrane of the bacteria during the contact interaction. Comparing Figures 4 and 5 shows that the effluxes of RNA from the *S. aureus* bacteria exposed to the nanowalls were considerably higher than the effluxes of the *E. coli* bacteria at the same conditions. This can be attributed to more resistance of the *E. coli* bacteria against the direct contact interaction with the edge of the nanowalls as compared to the *S. aureus* bacteria. Indeed, *S. aureus* as a Gram-positive bacterium is constituted by a peptidoglycan layer with a thickness ranging from 20 to 80 nm, without an outer membrane. However, although *E. coli* as a Gram-negative bacterium has a much thinner layer of peptidoglycan (thickness of 7−8 nm), it possesses an additional layer, that is, the outer membrane. It was also previously reported that *E. coli* exhibited more resistance to a direct contact interaction induced by an AFM tip than *S. aureus*, due to the outer membrane of the Gram-negative *E. coli* bacteria.[53] Here, it was found that the direct contact interaction of the bacteria with the very sharp edge of the nanowalls resulted in more damage to the cell membrane of the Gram-positive *S. aureus* bacteria lacking the outer membrane as compared to the Gram-negative *E. coli* ones owning the outer membrane.

CONCLUSIONS

The GONWs were achieved by EPD of Mg^{2+}-graphene oxide nanosheets synthesized by a chemical exfoliation procedure. In addition to SEM images of the nanowalls, Raman spectroscopy confirmed that the deposited GONWs constituted by single- and multi-layer graphene oxide sheets. The efflux of RNA of the bacteria indicated that the cell membrane of the bacteria was effectively damaged by direct contact of the bacteria with the very sharp edges of the nanowalls, resulting in inactivation of the bacteria by the nanowalls. The RNA efflux showed that the cell membrane of *S. aureus* bacteria was further damaged as compared to cell membrane damage of *E. coli*. The more resistance of the *E. coli* bacteria against the direct contact interaction with the nanowalls as compared to the *S. aureus* bacteria was assigned to the existence of an outer membrane in the structure of Gram-negative *E. coli* bacteria and the lack of such an outer membrane in the structure of Gram-positive *S. aureus* bacteria. The GONWs reduced by hydrazine exhibited more antibacterial activity as compared to the unreduced GONWs. The higher bacterial toxicity of the reduced nanowalls was attributed to more sharpening of the edges of the nanowalls providing stronger contact interaction with the cell membrane and/or better charge transfer between the bacteria and the reduced nanowalls, resulting in more cell membrane damage of the bacteria.

EXPERIMENTAL SECTION

Preparation of Graphene Oxide Nanosheets. The modified Hummers method[54,55] was utilized to oxidize natural graphite powders (45 μm, Sigma-Aldrich). In this method, 50 mL of H_2SO_4 was added into a beaker containing 2 g of graphite at room temperature. The beaker was cooled to 0 °C by using an ice bath. Then, 6 g of potassium permanganate ($KMnO_4$) was slowly added to the above mixture while it was allowed to warm to room temperature. The suspension was stirred for 2 h at 35 °C. After the suspension was cooled in an ice bath, it was diluted by 350 mL of deionized (DI) water. Then, H_2O_2 (30%) was added until the gas evolution ceased in order to be sure about reduction of residual permanganate to soluble manganese ions. The achieved suspension was filtered, washed by DI water, and dried at 60 °C for 24 h to obtain brownish graphite oxide powder. The graphite oxide powder was thermally exfoliated by rapidly heating the powder in a tube furnace. After the furnace was heated to 1050 °C, an alumina boat loaded with the graphite oxide was quickly moved into the heating zone of the furnace, kept there for 30 s, and rapidly removed from there.

Deposition of Graphene Nanowalls. At first a graphene oxide suspension was prepared by dispersing the obtained graphene oxide powder (1 mg/mL) in isopropyl alcohol. Then, $Mg(NO_3)_2 \cdot 6H_2O$ as charger was added to the suspension in order to achieve the graphene sheets positively charged. The weight ratio of the graphene oxide to the magnesium nitrate

was identical. By using this method, a uniform and stable Mg^{2+}-graphene oxide sheet suspension was obtained as the electrolyte applicable in the EPD of the graphene oxide nanosheets. Two polished stainless steel substrates were used as electrodes. The distance between the two electrodes was about 5 mm, and the applied voltage of 150 V was selected. By applying the voltage, the positively charged graphene oxide sheets were moved toward the negative electrode, and subsequently, were deposited on its surface. Here, the deposition time was considered 2 min to obtain the GONWs on the stainless steel substrate. Some of the prepared GONWs were also reduced by hydrazine vapor for 1 h.

Material Characterization. Surface morphology of the GONWs was studied by using a field-emission SEM operating at 5 kV (JSM 6500F; JEOL). XPS was utilized to study the changes that occurred in chemical states of the graphene oxides. The data were acquired by using a hemispherical analyzer equipped with a monochromatic Al Kα X-ray source ($h\nu = 1486.6$ eV) operating at a vacuum better than 10^{-7} Pa. The XPS peaks were deconvoluted by using Gaussian components after a Shirley background subtraction. Raman spectroscopy was performed at room temperature with a Raman Microprobe (HR-800 Jobin-Yvon) with 532 nm Nd:YAG excitation source to examine the change in the carbon structure of the GONWs.

Antimicrobial Test. With use of the so-called antibacterial drop-test, the bactericidal activities of all the samples were investigated against *E. coli* (ATCC 25922) and *S. aureus* (ATCC 25923) bacteria as Gram-negative and Gram-positive models, respectively. Before each microbiological experiment, all the samples and glassware were sterilized by autoclaving at 120 °C for 10 min. The bacteria were cultured on a nutrient agar plate at 37 °C for 24 h. Then, the cultured bacteria were added in 10 mL of saline solution to reach the concentration of bacteria of ~10^8 colony forming units per milliliter (CFU/mL). A portion of the bacterial suspension was diluted to 10^6 CFU/mL. For the antibacterial drop-test, each sample was placed into a sterilized Petri dish. Then, 100 µL of the diluted bacterial suspension was spread on surface of the sample. After sonication of the sample for 60 min at 37 °C, the bacteria were washed from the surface of the sample with 5 mL of PBS in the sterilized Petri dish. Then, 100 µL of each bacterial suspension was spread on a nutrient agar plate and incubated at 37 °C for 24 h to count the surviving bacterial colonies by using an optical microscope. The total number of the cells forming unit was determined by area based estimation. The reported data were the average value of three separate similar runs.

Measurement of Efflux of RNA. At first, the PBS remaining from the antibacterial test of each sample was diluted to 50 mL. Then, the solution was centrifuged at 2000 rev/min for 10 min. After that, a vial tube with 50 µL of β-mercaptoethanol was loaded by 10 mL of the supernatant of the solution. RNA of the bacteria was separated using a RNA purification kit and measured with a NanoDrop ND-1000 spectrophotometer.

REFERENCES AND NOTES

1. Zhang, Y. B.; Tan, Y.; Stormer, H. L.; Kim, P. Experimental Observation of Quantum Hall Effect and Berry's Phase In Graphene. *Nature* **2005**, *438*, 201–204.
2. Katsnelson, M. I.; Novoselov, K. S. Graphene: New Bridge Between Condensed Matter Physics and Quantum Electrodynamics. *Solid State Commun.* **2007**, *143*, 3–13.
3. Novoselov, K. S.; Geim, A. K.; Morozov, S. V.; Jiang, D.; Katsnelson, M. I.; Grigorieva, I. V.; Dubonos, S. V.; Firsov, A. A. Two-Dimensional Gas of Massless Dirac Fermions In Graphene. *Nature* **2005**, *438*, 197–200.
4. Meyer, J. C.; Geim, A. K.; Katsnelson, M. I.; Novoselov, K. S.; Booth, T. J.; Roth, S. The Structure of Suspended Graphene Sheets. *Nature* **2007**, *446*, 60–63.
5. Wu, Z.-S.; Pei, S.; Ren, W.; Tang, D.; Gao, L.; Liu, B.; Li, F.; Liu, C.; Cheng, H.-M. Field Emission of Single-Layer Graphene Films Prepared by Electrophoretic Deposition. *Adv. Mater.* **2009**, *21*, 1756–1760.
6. Shang, N. G.; Papakonstantinou, P.; McMullan, M.; Chu, M.; Stamboulis, A.; Potenza, A.; Dhesi, S. S. Marchetto-Free Efficient Growth, Orientation and Biosensing Properties of Multilayer Graphene Nanoflake Films with Sharp Edge Planes. *Adv. Funct. Mater.* **2008**, *18*, 3506–3514.
7. Bai, J.; Zhong, X.; Jiang, S.; Huang, Y.; Duan, X. Graphene Nanomesh. *Nat. Nanotechnol.* **2010**, *5*, 190–194.
8. Akhavan, O. Graphene Nanomesh by ZnO Nanorod Photocatalysts. *ACS Nano* **2010**, *4*, 4174–4180.
9. Akhavan, O.; Abdolahad, M.; Esfandiar, A.; Mohatashamifar, M. Photodegradation of Graphene Oxide Sheets by TiO$_2$ Nanoparticles After a Photocatalytic Reduction. *J. Phys. Chem. C* **2010**, *114*, 12955–12959.
10. Schedin, F.; Geim, A. K.; Morozov, S. V.; Hill, E. W.; Blake, P.; Katsnelson, M. I.; Novoselov, K. S. Detection of Individual Gas Molecules Adsorbed on Graphene. *Nat. Mater.* **2007**, *6*, 652–655.
11. Gomez-Navarro, C.; Weitz, R. T.; Bittner, A. M.; Scolari, M.; Mews, A.; Burghard, M.; Kern, K. Electronic Transport Properties of Individual Chemically Reduced Graphene Oxide Sheets. *Nano Lett.* **2007**, *7*, 3499–3503.
12. Liang, X.; Fu, Z.; Chou, S. Y. Graphene Transistors Fabricated via Transfer-Printing In Device Active-Areas on Large Wafer. *Nano Lett.* **2007**, *7*, 3840–3844.
13. Gilje, S.; Han, S.; Wang, M.; Wang, K. L.; Kaner, R. B. A Chemical Route to Graphene for Device Applications. *Nano Lett.* **2007**, *7*, 3394–3398.
14. Robinson, J. T.; Perkins, F. K.; Snow, E. S.; Wei, Z. Q.; Sheehan, P. E. Reduced Graphene Oxide Molecular Sensors. *Nano Lett.* **2008**, *8*, 3137–3140.
15. Wang, X.; Zhi, L. J.; Tsao, N.; Tomovic, Z.; Li, J. L.; Mullen, K. Transparent Carbon Films As Electrodes In Organic Solar Cells. *Angew Chem., Int. Ed.* **2008**, *47*, 2990–2992.
16. Stampfer, C.; Schurtenberger, E.; Molitor, F.; Güttinger, J.; Ihn, T.; Ensslin, K. Tunable Graphene Single Electron Transistor. *Nano Lett.* **2008**, *8*, 2378–2383.
17. Bao, W.; Zhang, H.; Bruck, J.; Lau, C. N.; Bockrath, M.; Standley, B. Graphene-Based Atomic-Scale Switches. *Nano Lett.* **2008**, *8*, 3345–3349.
18. Arsat, R.; Breedon, M.; Shafiei, M.; Spizziri, P. G.; Gilje, S.; Kaner, R. B.; Kalantar-zadeh, K.; Wlodarski, W. Graphene-Like Nano-Sheets for Surface Acoustic Wave Gas Sensor Applications. *Chem. Phys. Lett.* **2009**, *467*, 344–347.
19. Mohanty, N.; Berry, V. Graphene-Based Single-Bacterium Resolution Biodevice and DNA Transistor: Interfacing Graphene Derivatives with Nanoscale and Microscale Biocomponents. *Nano Lett.* **2008**, *8*, 4469–4476.
20. Hong, W.; Bai, H.; Xu, Y.; Yao, Z.; Gu, Z.; Shi, G. Preparation of Gold Nanoparticle/Graphene Composites with Controlled Weight Contents and Their Application In Biosensors. *J. Phys. Chem. C* **2010**, *114*, 1822–1826.
21. Choi, B. G.; Park, H. S.; Park, T. J.; Yang, M. H.; Kim, J. S.; Jang, S.-Y.; Heo, N. S.; Lee, S. Y.; Kong, J.; Hong, W. H. Solution Chemistry of Self-Assembled Graphene Nanohybrids for High-Performance Flexible Biosensors. *ACS Nano* **2010**, *4*, 2910–2918.
22. Shvedova, A. A.; Castranova, V.; Kisin, E. R.; Schwegler-Berry, D.; Murray, A. R.; Gandelsman, V. Z.; Maynard, A.; Baron, P. Exposure to Carbon Nanotube Material: Assessment of Nanotube Cytotoxicity Using Human Keratinocyte Cells. *J. Toxicol. Environ. Health, Part A* **2003**, *66*, 1909–1926.
23. Manna, S. K.; Sarkar, S.; Barr, J.; Wise, K.; Barrera, E. V.; Jejelowo, O.; Rice-Ficht, A. C.; Ramesh, G. T. Single-Walled Carbon Nanotube Induces Oxidative Stress and Activates Nuclear Transcription Factor-κB In Human Keratinocytes. *Nano Lett.* **2005**, *5*, 1676–1684.
24. Ding, L. H.; Stilwell, J.; Zhang, T. T.; Elboudwarej, O.; Jiang, H. J.; Selegue, J. P.; Cooke, P. A.; Gray, J. W.; Chen, F. F. Molecular Characterization of the Cytotoxic Mechanism of Multiwall Carbon Nanotubes and Nano-Onions on Human Skin Fibroblast. *Nano Lett.* **2005**, *5*, 2448–2464.

25. Magrez, A.; Kasas, S.; Salicio, V.; Pasquier, N.; Seo, J. W.; Celio, M.; Catsicas, S.; Schwaller, B.; Forr, L. Cellular Toxicity of Carbon-Based Nanomaterials. *Nano Lett.* **2006**, *6*, 1121–1125.

26. Jia, G.; Wang, H. F.; Yan, L.; Wang, X.; Pei, R. J.; Yan, T.; Zhao, Y. L.; Guo, X. B. Cytotoxicity of Carbon Nanomaterials: Single-Wall Nanotube, Multi-Wall Nanotube, and Fullerene. *Environ. Sci. Technol.* **2005**, *39*, 1378–1383.

27. Lam, C. W.; James, J. T.; McCluskey, R.; Hunter, R. L. Pulmonary Toxicity of Single-Wall Carbon Nanotubes In Mice 7 and 90 Days After Intratracheal Instillation. Toxicol. *Science* **2004**, *77*, 126–134.

28. Chen, X.; Tam, U. C.; Czlapinski, J. L.; Lee, G. S.; Rabuka, D.; Zettl, A.; Bertozzi, C. R. Interfacing Carbon Nanotubes with Living Cells. *J. Am. Chem. Soc.* **2006**, *128*, 6292–6293.

29. Akhavan, O.; Abdolahad, M.; Abdi, Y.; Mohajerzadeh, S. Synthesis of Titania/Carbon Nanotubes Heterojunction Arrays for Photoinactivation of *E. coli* In Visible Light Irradiation. *Carbon* **2009**, *47*, 3280–3287.

30. Nel, A.; Xia, T.; Madler, L.; Li, N. Toxic Potential of Materials at the Nanolevel. *Science* **2006**, *311*, 622–627.

31. Pulskamp, K.; Diabate, S.; Krug, H. F. Carbon Nanotubes Show No Sign of Acute Toxicity But Induce Intracellular Reactive Oxygen Species In Dependence on Contaminants. *Toxicol. Lett.* **2007**, *168*, 58–74.

32. Narayan, R. J.; Berry, C. J.; Brigmon, R. L. Structural and Biological Properties of Carbon Nanotube Composite Films. *Mater. Sci. Eng., B* **2005**, *123*, 123–129.

33. Kang, S.; Pinault, M.; Pfefferle, L.; Elimelech, M. Single-Walled Carbon Nanotubes Exhibit Strong Antimicrobial Activity. *Langmuir* **2007**, *23*, 8670–8673.

34. Boor, K. J. Bacterial Stress Responses: What Doesn't Kill Them Can Make Them Stronger. *PLoS. Biol.* **2006**, *4*, 18–20.

35. Kang, S.; Herzberg, M.; Rodrigues, D. F.; Elimelech, M. Antibacterial Effects of Carbon Nanotubes: Size Does Matter! *Langmuir* **2008**, *24*, 6409–6413.

36. Chen, H.; Müller, M. B.; Gilmore, K. J.; Wallace, G. G.; Li, D. Mechanically Strong, Electrically Conductive, and Biocompatible Graphene Paper. *Adv. Mater.* **2008**, *20*, 3557–3561.

37. Park, S.; Mohanty, N.; Suk, J. W.; Nagaraja, A.; An, J.; Piner, R. D.; Cai, W.; Dreyer, D. R.; Berry, V.; Ruoff, R. S. Biocompatible, Robust Free-Standing Paper Composed of a TWEEN/Graphene Composite. *Adv. Mater.* **2010**, *22*, 1736–1740.

38. Hu, W.; Peng, C.; Luo, W.; Lv, M.; Li, X.; Li, D.; Huang, Q.; Fan, C. Graphene-Based Antibacterial Paper. *ACS Nano* **2010**, *4*, 4317–4323.

39. Akhavan, O.; Ghaderi, E. Photocatalytic Reduction of Graphene Oxide Nanosheets on TiO₂ Thin Film for Photoinactivation of Bacteria In Solar Light Irradiation. *J. Phys. Chem. C* **2009**, *113*, 20214–20220.

40. Gao, B.; Yue, G. Z.; Qiu, Q.; Cheng, Y.; Shimoda, H.; Fleming, L.; Zhou, O. Fabrication and Electron Field Emission Properties of Carbon Nanotube Films by Electrophoretic Deposition. *Adv. Mater.* **2001**, *13*, 1770–1773.

41. Jung, S. M.; Hahn, J.; Jung, H. Y.; Suh, J. S. Clean Carbon Nanotube Field Emitters Aligned Horizontally. *Nano Lett.* **2006**, *6*, 1569–1573.

42. Wu, Z.-S.; Pei, S.; Ren, W.; Tang, D.; Gao, L.; Liu, B.; Li, F.; Liu, C.; Cheng, H.-M. Field Emission of Single-Layer Graphene Films Prepared by Electrophoretic Deposition. *Adv. Mater.* **2009**, *21*, 1756–1760.

43. Akhavan, O. The Effect of Heat Treatment on Formation of Graphene Thin Films from Graphene Oxide Nanosheets. *Carbon* **2009**, *48*, 509–519.

44. Yang, D.; Velamakanni, A.; Bozoklu, G.; Park, S.; Stoller, M.; Piner, R. D.; Stankovich, S.; Jung, I.; Field, D. A., Jr.; Ruoff, R. S. Chemical Analysis of Graphene Oxide Films After Heat and Chemical Treatments by X-Ray Photoelectron and Micro-Raman Spectroscopy. *Carbon* **2009**, *47*, 145–152.

45. Chiang, T. C.; Seitz, F. Photoemission Spectroscopy In Solids. *Ann. Phys.* **2001**, *10*, 61–74.

46. Yumitori, S. Correlation of C1s Chemical State Intensities with the O1s Intensity In the XPS Analysis of Anodically Oxidized Glass-Like Carbon Samples. *J. Mater. Sci.* **2000**, *35*, 139–146.

47. Ferrari, A. C.; Robertson, J. Interpretation of Raman Spectra of Disordered and Amorphous Carbon. *Phys. Rev. B* **2000**, *61*, 14095–14107.

48. Graf, D.; Molitor, F.; Ensslin, K.; Stampfer, C.; Jungen, A.; Hierold, C.; Wirtz, L. Spatially Resolved Raman Spectroscopy of Single- and Few-Layer Graphene. *Nano Lett.* **2007**, *7*, 238–242.

49. Kudin, K. N.; Ozbas, B.; Schniepp, H. C.; Prud'homme, R. K.; Aksay, I. A.; Car, R. Raman Spectra of Graphite Oxide and Functionalized Graphene Sheets. *Nano Lett.* **2008**, *8*, 36–41.

50. Dato, A.; Radmilovic, V.; Lee, Z.; Phillips, J.; Frenkach, M. Substrate Free Gas-Phase Synthesis of Graphene Sheets. *Nano Lett.* **2008**, *8*, 2012–2016.

51. Ferrari, A. C.; Meyer, J. C.; Scardaci, V.; Casiraghi, C.; Lazzeri, M.; Mauri, F.; Piscanec, S.; Jiang, D.; Novoselov, K. S.; Roth, S.; Geim, A. K. The Raman Fingerprint of Graphene and Graphene Layers. *Phys. Rev. Lett.* **2006**, *97*, 187401.

52. Calizo, I.; Balandin, A. A.; Bao, W.; Miao, F.; Lau, C. N. Temperature Dependence of the Raman Spectra of Graphene and Graphene Multilayers. *Nano Lett.* **2007**, *7*, 2645–2649.

53. Eaton, P.; Fernandes, J. C.; Pereira, E.; Pintado, M. E.; Malcata, F. X. Atomic Force Microscopy Study of the Antibacterial Effects of Chitosans on *Escherichia coli* and *Staphylococcus aureus*. *Ultramicroscopy* **2008**, *108*, 1128–1134.

54. Hummers, W. S.; Offeman, R. E. Preparation of Graphitic Oxide. *J. Am. Chem. Soc.* **1958**, *80*, 1339.

55. Stankovich, S.; Dikin, D. A.; Piner, R. D.; Kohlhaas, K. A.; Kleinhammes, A.; Jia, Y.; Wu, Y.; Nguyen, S. T.; Ruoff, R. S. Synthesis of Graphene-Based Nanosheets via Chemical Reduction of Exfoliated Graphite Oxide. *Carbon* **2007**, *45*, 1558a1565.